Check for updates

ADVANCING EARTH AND SPACE SCIENCES

Geophysical Research Letters

RESEARCH LETTER
10.1029/2024GL114362

Key Points:

- We present evidence for petit-spot volcanism on the eastern section of the outer rise of the Puerto Rico Trench
- Faults scarps are longer and higher in the eastern section versus the equally well mapped section to the west
- The enhanced faulting in the east may provide a melt pathway for the petit-spot volcanism

Correspondence to:
N. Harmon,
nicholas.harmon@whoi.edu

Citation:
Harmon, N., Danforth, W., Ten Brink, U., Canales, J. P., Han, S., Vanacore, E., et al. (2025). Evidence for petit-spot volcanism in the Puerto Rico Trench. *Geophysical Research Letters*, *52*, e2024GL114362. https://doi.org/10.1029/2024GL114362

Received 20 DEC 2024
Accepted 2 APR 2025

Author Contributions:
Conceptualization: Nicholas Harmon
Data curation: Jose-Luis Granja-Bruña, Wayne Baldwin, Seth Ackerman, Liam Moser, Elisaveta Sokolkova
Formal analysis: Nicholas Harmon, William Danforth, Uri Ten Brink, J. Pablo Canales, Shuoshuo Han, Elizabeth Vanacore, Jose-Luis Granja-Bruña, Seth Ackerman, Liam Moser, Elisaveta Sokolkova
Funding acquisition: Uri Ten Brink, J. Pablo Canales, Shuoshuo Han, Elizabeth Vanacore
Methodology: Nicholas Harmon, William Danforth, Wayne Baldwin, Seth Ackerman, Liam Moser
Validation: Wayne Baldwin
Writing – original draft: Nicholas Harmon
Writing – review & editing: Nicholas Harmon, William Danforth, Uri Ten Brink, J. Pablo Canales, Shuoshuo Han, Elizabeth Vanacore, Jose-Luis Granja-Bruña, Liam Moser, Elisaveta Sokolkova

© 2025. The Author(s).
This is an open access article under the terms of the Creative Commons Attribution License, which permits use, distribution and reproduction in any medium, provided the original work is properly cited.

Evidence for Petit-Spot Volcanism in the Puerto Rico Trench

Nicholas Harmon[1], William Danforth[2], Uri Ten Brink[2], J. Pablo Canales[1], Shuoshuo Han[3], Elizabeth Vanacore[4], Jose-Luis Granja-Bruña[5], Wayne Baldwin[2], Seth Ackerman[2], Liam Moser[1,6], and Elisaveta Sokolkova[7]

[1]Geology and Geophysics, Woods Hole Oceanographic Institution, Woods Hole, MA, USA, [2]United States Geological Survey, Woods Hole, MA, USA, [3]Institute for Geophysics, University of Texas, Austin, TX, USA, [4]University of Puerto Rico, Mayaguez, PR, USA, [5]Universidad Complutense de Madrid, Madrid, Spain, [6]Earth and Planetary Science, Massachusetts Institute of Technology, Cambridge, MA, USA, [7]GEOMAR Helmholtz Centre for Ocean Research, Kiel, Germany

Abstract Petit-spot volcanism occurs in intraplate settings along the outer rise of subducting plates. Here we present evidence for petit-spot type of volcanism from multibeam bathymetry and backscatter data from the Puerto Rico Trench (PRT). It is the first report of such volcanism in the Atlantic basin. Up to 34 possible petit-spot volcanic cones are mapped in the eastern section of the PRT, with an average diameter of 950 m and a mean height of 92 m. The seamounts are in a region of the PRT that has the longest and highest bending faults, up to 50.6 km long and 1.49 km high. Some of the volcanic cones are associated with fault scarps. The larger bending fault scarps in the region of the volcanic cones suggest the stress state in the eastern PRT is favorable for allowing asthenospheric melt to escape to the surface.

Plain Language Summary Plate tectonic theory explains most of the places where volcanos occur on Earth, like the mid-ocean ridges and hot spots like Hawaii. “Petit-spot” volcanos are special because they occur where the tectonic plates are bending and breaking near deep ocean trenches, and pre-existing ambient melt in the mantle escapes through the cracks. Due to this unique process, the petit-spots offer a glimpse into the chemistry and melting dynamics of the ambient mantle beneath tectonic plates that is not over printed by the aforementioned large-scale plate tectonic melting processes. In this paper we present evidence for petit-spot volcanism and associated faulting based on echo sounder mapping of the seafloor offshore Puerto Rico, USA. This is the first evidence for this type of volcano in the Atlantic and will lead to future studies sampling these volcanos to understand mantle convection and chemistry.

1. Introduction

Plate tectonic theory can explain most of the volcanism on Earth but not all. Adiabatic decompression melting caused by plate spreading explains mid-ocean ridge volcanism (Forsyth, 1992; Klein & Langmuir, 1987), while flux melting caused by dehydration of subduction plates explains arc volcanism (Stern, 2002). Hot and/or chemically enriched mantle plumes cause super-adiabatic decompression melting which generate large volcanic islands such as the Hawaii-Emperor seamount chain with age increasing in the absolute plate motion direction (Morgan, 1971). However, there are numerous locations in intraplate settings that have volcanism with no clear age progression (e.g., Hirano et al., 2006; Sandwell et al., 1995). In these locations, processes besides large-scale mantle convection/plate tectonics are needed to explain magma genesis.

Petit-spot volcanism is a type of non-hotspot intraplate volcanism associated with the outer rise of subducting plates (Hirano et al., 2006). The hypothesis to explain the magmatism is that pre-existing asthenospheric melt is released to the surface through flexural faulting of the outer rise (Hirano et al., 2006). Further numerical modeling work demonstrates that ambient melt ponded at the lithosphere-asthenosphere boundary (LAB) may be quickly extracted via cracking of the lithosphere under flexural stress (Yamamoto et al., 2014). The hypothesis is consistent with numerous geophysical observations of inferred melt at the LAB in intraplate oceanic settings (Mehouachi & Singh, 2018; Naif et al., 2013; Rychert et al., 2020; Rychert & Shearer, 2011; Wang et al., 2020). Although initially observed near the Japan Trench (Hirano, 2011; Hirano et al., 2006), other sites of petit-spot volcanism have been found off the Chile Trench (Hirano et al., 2013), Mariana Trench (Hirano et al., 2019; Peretyazhko et al., 2024) and the Sunda Trench (Taneja et al., 2016). Petit-spot magmas have a unique composition, with evidence for metasomatism as the melts traversed and stalled in the lithosphere (Pilet

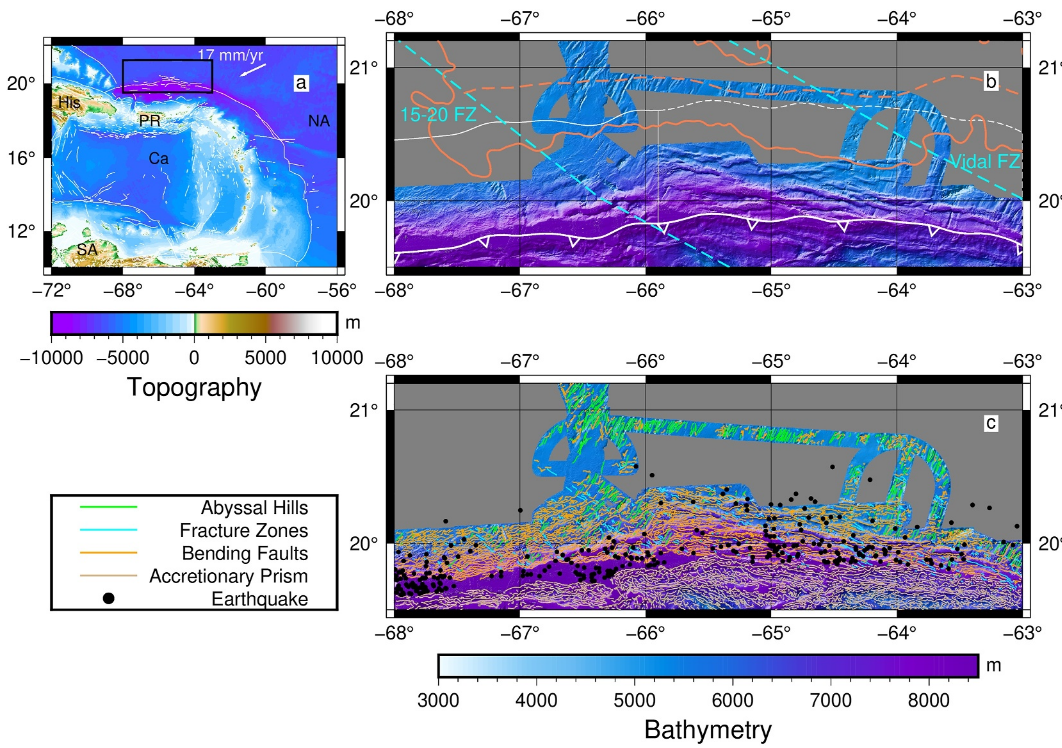

Figure 1. Location and bathymetry of the northern Puerto Rico Trench (PRT). (a) General area map of the eastern Caribbean subduction zone. White lines indicate major fault systems in the region (French & Schenk, 2004). Arrow indicates the convergence between the North American and the Caribbean plates. Labels are as follows: Ca, Caribbean Plate; NA, North American Plate; SA, South American Plate; PR, Puerto Rico, His-Hispaniola Island. Box indicates location of our study area in the northern PRT. (b) Uninterpreted bathymetry. White front line shows trench axis based on the deepest location of the trench. White solid line shows western section of the PRT outer rise, and the white dashed line shows the eastern section. Blue dashed lines show trends of large offset fracture zones in the region from a recent plate motion model (Matthews et al., 2016). Coral contour shows the 0 mGal contour of the free-air gravity anomaly (Sandwell et al., 2014) to highlight the extent of the outer rise, and the dashed orange line shows the inferred axis of the outer rise. (c) Interpreted bathymetry, legend indicates the colors of the different fault types and earthquakes (USGS, 2024).

et al., 2016), and high amounts of CO_2 (>5%) and water (>1%) (Machida et al., 2017; Okumura & Hirano, 2013). Petit-spots alter the local crustal structure beneath the volcanic edifices, disturbing the seafloor sediments (Akizawa et al., 2022; Fujiwara et al., 2007) and reducing the seismic velocity of the basement relative to the surrounding region, attributed to dike and sill emplacement and associated cracking and faulting (Ohira et al., 2018). To date no upper mantle imaging of the LAB beneath petit-spot volcanism has been performed to determine if ponded melt is the mantle source. Although not voluminous, petit-spot volcanics may sample normal oceanic asthenosphere and lithosphere through mantle derived magmas and xenoliths (Harigane et al., 2011; Mikuni et al., 2022). This provides a unique glimpse into the state of the mantle away from hotspots, ridges and subduction zones (Hirano & Machida, 2022; Machida et al., 2017).

While petit-spot volcanism has been observed in many places in the Pacific and in the Indian ocean basins, to date there have been no observations in the Atlantic basin, which has only two subduction systems. Here we focus on the Greater/Lesser Antilles subduction zone, specifically, the PRT, where we have recently acquired new bathymetric data on the outer rise. At the PRT the North American Plate is subducting obliquely at ∼240–250° azimuth beneath the Caribbean plate at ∼17–20 mm/yr (Altamimi et al., 2023; DeMets et al., 2010; Symithe et al., 2015). The subducting plate in our study area is 99–115 Myr old and was generated at the Mid-Atlantic Ridge (Muller et al., 2008) (Figure 1a). Estimates of the North American Plate thickness from S-to-P receiver functions north of the nearby island of Hispaniola range from 90 to 100 km (Possee et al., 2021). However, the S-to-P study did not detect a significant LAB phase north of Puerto Rico (Possee et al., 2021), although there was limited depth resolution due to the data coverage. Bend faulting on the outer rise is pronounced in some sections due to trench collapse which has contributed to generating the deepest part of the Atlantic Ocean in the PRT (ten

19448007, 2025, 10, Downloaded from https://agupubs.onlinelibrary.wiley.com/doi/10.1029/2024GL114362 by Universidad Complutense De Madrid, Wiley Online Library on [09/02/2026]. See the Terms and Conditions (https://onlinelibrary.wiley.com/terms-and-conditions) on Wiley Online Library for rules of use; OA articles are governed by the applicable Creative Commons License

10.1029/2024GL114362

Brink, 2005; ten Brink et al., 2004). The faulting may also contribute to the thinner than expected effective elastic thickness determined for some parts of the system (Levitt & Sandwell, 1995).

In this paper we present evidence from multibeam bathymetry and backscatter intensity for possible petit-spot volcanism on the outer rise of the PRT. We map scarps across the region to establish if there is a relationship between the locations of possible petit-spot volcanism and fault scarp parameters. The aim is to determine if there is a genetic relationship or if fault scarp parameters suggest a favorable stress regime for volcanism in general. We also examine the spatial relationship between the possible petit-spots and the outer rise. The goal of this paper is to present this information for future in-situ sampling efforts.

2. Methods

The bathymetry presented in this paper is a compilation of data collected during several cruises on the NOAA Ship Ronald Brown (RB0208, RB0303, RB0305, RB0604) between 2002–2006 and the RV Marcus G. Langseth (MGL2315, MGL2316) in 2023. Data from the Ronald Brown were presented in earlier work and details of the processing are provided therein (Andrews et al., 2014; ten Brink et al., 2004). The RV Langseth data are from a Kongsberg EM122 multibeam echo sounder and are processed using QPS Qimera software. Daily sound velocity profiles of the upper ∼1,000 m from expendable bathy-thermographs coupled with a global atlas of sound velocity at greater depth (Antonov et al., 2010; Levitus, 1982; Locarnini et al., 2010) are incorporated into the processing workflow. The ship's soundings are taken relative to the ship's GPS which accounted for tidal height variations. The soundings are filtered using a spline filter, and then hand edited to remove spurious soundings. The soundings are then gridded onto a $0.1' \times 0.1'$ (185.2×185.2 m) grid aligned with the Ronald Brown data. Backscatter data from the RV Langseth are processed using QPS FMGT software and gridded onto a 25×25 m grid. We do not use backscatter data from the Ronald Brown here.

Cross over analysis (e.g., Wessel, 1989) is performed between the Ronald Brown and RV Langseth bathymetry data by examining the differences between common grid cells prior to merging the two data sets. The bias (static shift) between the two data sets is removed from the RV Langseth data. Where the two data sets have common grid cells the two data sets are merged by preferentially taking the RV Langseth data over the Ronald Brown data.

We map two types of features: scarps, which are associated with faulting, and small seamounts or knolls (used hereafter), which may be regions of recent volcanism. For the scarp mapping we use a semi-automated workflow. We first employ a "Canny" edge detection algorithm (Canny, 1986) on the bathymetry grid using MATLAB software. The edge detection algorithm first smooths the data with a 2-D Gaussian filter, followed by the detection of high local gradients. The local gradient points are then subjected to double thresholding, where points above a maximum threshold are classed as edges, points between the upper and lower thresholds are classed as possible edges and points below the lower threshold are rejected as edges. Then a winnowing of spatially close edge points is performed based on their threshold values to remove clusters of points and yield a single edge "line" of points. Edge points associated with bathymetric artifacts such as trackline edges caused by merging data sets are removed. Edge points are then associated into individual scarps by grouping points that are immediately adjacent to each other using the eight-point stencil around each grid point. Each individual scarp is then fit with a 20-segment smooth spline. Scarps less than 500 m long are removed from further consideration. The spline is used for determining median azimuth and total scarp length. Scarp heights are determined for each of the 20 spline segments by projecting the bathymetry and gradient magnitude data perpendicular to the trend of the segment. The segment scarp height is determined from the average difference between the bathymetry points corresponding to the minima in gradient magnitude on either side of the local maximum gradient magnitude associated with the scarp. These minima correspond to where the bathymetry "flattens" out on either side of the slope. When there is a local bench on the scarp, our scarp height measurement will estimate the height up to the local bench, resulting in a minimal estimate. Segments with insufficient data (e.g., very short segments) are not incorporated in the scarp height calculations.

Knoll locations are determined by visual inspection of the bathymetric and backscatter intensity data. Knolls with conical or hemispheric expressions are selected. We consider a knoll to have formed recently if the backscatter intensity is >100, because we interpret this intensity to be high enough to be rough sediment free hard-rock seafloor. The backscatter intensity is normalized between overlain tracks in a given mosaic to a grayscale between 0 and 255, so our choice is based on a relative scale for the local mosaic. Previous active source seismic studies show most of the seafloor has 100s m of pelagic sediments blanketing the surface (Bunce &

19448007, 2025, 10, Downloaded from https://agupubs.onlinelibrary.wiley.com/doi/10.1029/2024GL114362 by Universidad Complutense De Madrid, Wiley Online Library on [09/02/2026]. See the Terms and Conditions (https://onlinelibrary.wiley.com/terms-and-conditions) on Wiley Online Library for rules of use; OA articles are governed by the applicable Creative Commons License

19448007, 2025, 10, Downloaded from https://agupubs.onlinelibrary.wiley.com/doi/10.1029/2024GL114362 by Universidad Complutense De Madrid, Wiley Online Library on [09/02/2026]. See the Terms and Conditions (https://onlinelibrary.wiley.com/terms-and-conditions) on Wiley Online Library for rules of use; OA articles are governed by the applicable Creative Commons License

Fahlquist, 1962; Ewing & Ewing, 1962; Masson & Scanlon, 1991). Steep slopes can also cause high backscatter, so we limit the backscatter intensity selection to the tops of the knolls, where slopes are typically lower. We report the height of each knoll above the surrounding seafloor and the maximum radius of the edifice based on the break in slope.

3. Results

The new bathymetric data sets merged with the Ronald Brown data added 14,245 km^2 coverage to the area and extended coverage onto the outer rise. The PRT is visible at the deepest locations in the study region (Figure 1), with its axis along the greatest depths indicated with a white front line with a maximum depth of 8,518 m (Figures 1b and 1c). The outer rise lies to the north and at 65.9°W longitude there is a clear change in bending fault orientation in the bathymetric data and is near the change in trench axis orientation (Figures 1b and 1c). We use 65.9° W longitude to divide the outer rise into a western and eastern segment for further analysis of the scarps and possible petit-spot volcanic regions. In Figure 1 the solid white line delimits the western section, while the dashed white line delimits the eastern section.

Our semi-automated scarp mapping technique mapped 4,423 scarps north of our 19.5°N latitude cut-off. To classify scarps as being related to abyssal hills, pre-existing fracture zones or bending fault related scarps, we use azimuthal cut-offs. Abyssal hills are classified as scarps with a median azimuth between 0° and 50° (Figure 1c, green lines), while pre-existing fracture zones are classified as 110°–130° azimuth (Figure 1c, cyan lines). The fracture zone azimuth range (Figure 1b, dashed cyan lines) is determined from the trends of large offset fracture zones from a recent plate reconstruction model (Matthews et al., 2016). Bending faults are classified as the remainder of the scarps north of the trench axis (Figure 1c, orange lines). We classify all scarps that lie south of the PRT axis as being related to the accretionary prism and Bunce Fault strike slip system (Figure 1c, tan lines). This produced 656 abyssal hill scarps, 550 fracture zone scarps and 3,191 bending related faults within the outer rise area. There are 1,566 accretionary prism related scarps.

The histogram of all faults including fracture zones and abyssal hills mapped in the outer rise region shows a broad distribution of azimuths with a peak at centered at ∼90° (Figure 2a). The azimuthal distribution of the bending fault scarps varies between the east and west segments. The eastern section has 1,507 scarps, while the western section has 1,370 scarps. The eastern section has a mean azimuth of 91° with a well-defined peak in its histogram extending from 85° to 110°, while the western section has a broader distribution with no well-defined peak, with a mean of 81° (Figure 2a). The difference in the mean azimuth is statistically significant at the 95% confidence limit based on a *t*-test. We note that the eastern section azimuths are sub-parallel to the nominal trend of the area's fracture zones of 110°–130° azimuth. Scarp length and scarp height fall-off exponentially (Figures 2b and 2c) and co-vary in 2-D histograms (Figures 2d and 2e) as expected for fault systems (Kim & Sanderson, 2005; Torabi & Berg, 2011). The longest scarps are found within the eastern section, which has 46 scarps with >20 km length, while the western section has eight. The longest scarp is found in the eastern section at 50.6 km long although it extends into the western section by 5 km. The greatest scarp heights are also found in the eastern section, with a maximum segment height of 1,490 m in the east versus 970 m in the west. The largest average scarp height in the east is 1,012 m versus 598 m in the west.

Several knolls are visible in the eastern section of the outer rise of the PRT, while no knolls are visible in the western section (Figures 3 and 4). There are 59 knolls mapped in the eastern section (black and magenta circles Figure 3b). The knolls are typically small and have a conical to hemispherical morphology. Some are associated with scarps, while others are emerging through flat sedimented seafloor (Figures 3b and 3d; Figures 4b and 4d). The height above the median of the surrounding seafloor ranges from 17 to 208 m with an average of 92 m (Figure 2f). The knolls range from 170 to 1,180 m in radius, with a mean radius of 475 m (Figure 2g).

Several of the knolls have high backscatter intensity surrounding their edifices, while other knolls, with similar slopes have lower backscatter intensity (e.g., Figures 4a and 4c). Specifically, there are 34 seamounts with a backscatter intensity of >100 (magenta circles Figures 3b and 3d). We show a zoom of two knolls that emerge from relatively flat, presumably well sedimented seafloor (Bunce & Fahlquist, 1962) (Figures 4b and 4d). These knolls have high backscatter intensity and are the clearest examples of likely recent volcanism in the region. The knolls are located near a fault scarp with 90–100° azimuth, which are classified as bending faults here. The knolls seem to align along the azimuth of the faulting (Figure 3b, black box). However, we observe knolls with high backscatter intensity across the outer rise, north of where the outer rise is dominated by the bending faults (e.g.,

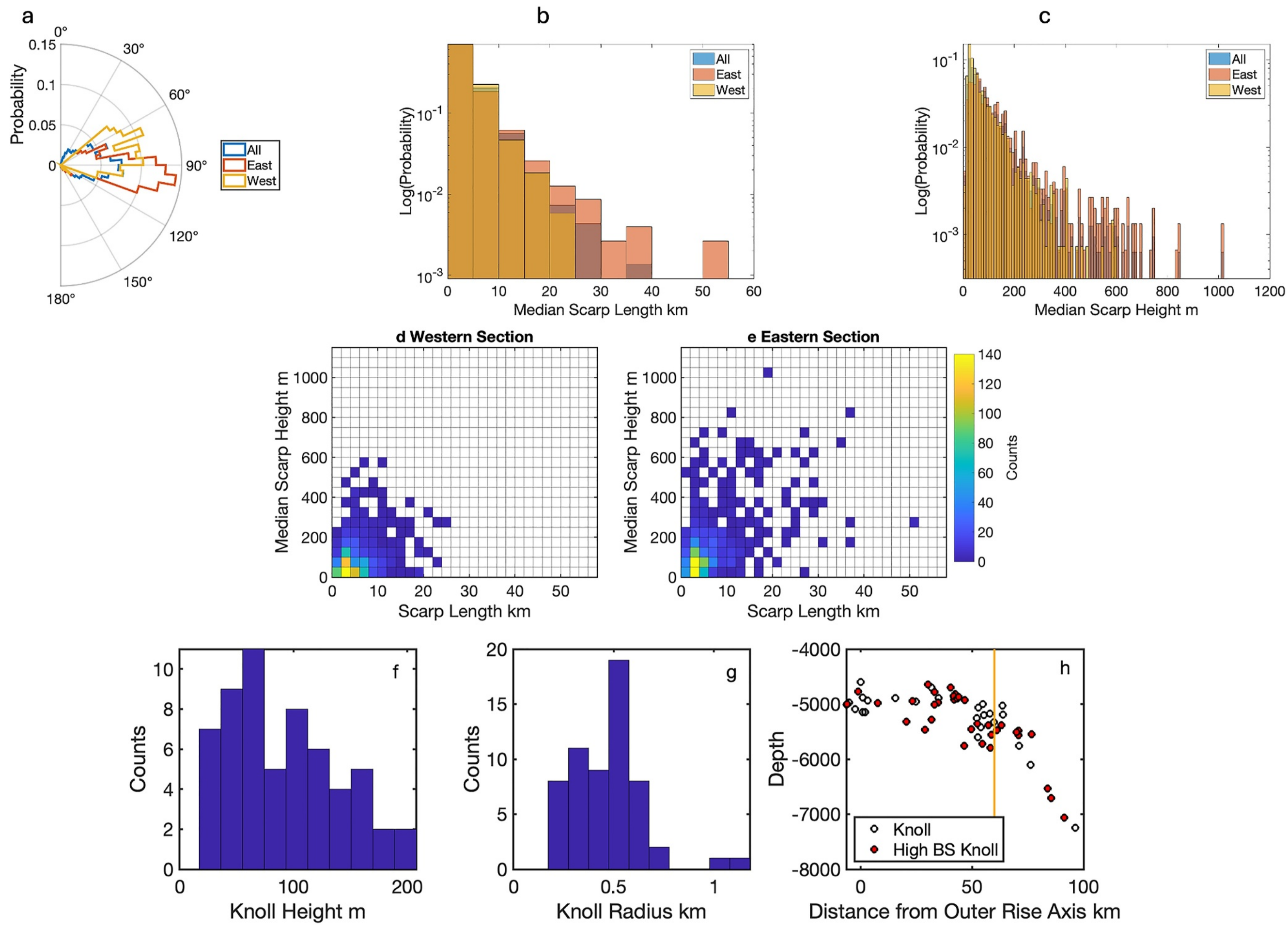

Figure 2. Histograms of scarp parameters: azimuth, length and height and seamount parameters height, radius and depth versus distance from outer rise axis (a) Histogram/rose diagram of mean scarp azimuth for the entire region (including fracture zone and abyssal hills) and the western and eastern sections. (b) Histogram of scarp length for the entire region and the western and eastern sections. (c) Histogram of median scarp height for the entire region and the western and eastern sections. (d) 2-D histogram of scarp length versus height for the western section and (e) 2-D histogram of scarp length versus height for the eastern section. (f) Histogram of knoll height, (g) Histogram of knoll radius, and (h) knoll depth versus distance from the outer rise axis, which is determined by the median latitude of the positive free-air gravity anomaly (FAA) above the outer rise (Figure 1). Orange line is at 60 km, the nominal extent of the positive FAA. High backscatter seamounts are shown with red symbols.

north of our eastern section region boundary). We observe 4 knolls with high backscatter intensity north of ~20.5°N (Figure 3d), before bending faulting becomes well developed, and 30 within the region of bending faulting. We also quantify the relative location of the knolls with respect to the axis of the outer rise (Figure 2h). We define the axis as the middle of the positive free-air gravity anomaly (FAA) associated with the outer rise (Figure 1b coral lines). The majority of knolls in the region (76%) lie within 60 km of the outer rise axis, that is, within the positive FAA, and 74% of the high back scatter intensity knolls lie within 60 km of the axis. The distribution of knolls relative to the outer rise axis should be interpreted with caution as there is a greater mapped area to the south.

4. Discussion

In comparison to other regions where petit-spot volcanism has been observed, the size and scale of volcanism at the PRT inferred from our analysis is consistent, and many of the high backscatter intensity seamounts are observed on the top of the flexural bulge and outer trench wall. Previous observations of petit-spot volcanism reveal small volcanic cones or flows that are 10–100s m high, and up to 1 km in radius (Hirano & Machida, 2022; Hirano et al., 2008), consistent with our observations. Many previously observed petit-spot volcanic areas occur seaward of the outer rise in the concave upward flexed regions of the incoming plate (Hirano & Machida, 2022;

19448007, 2025, 10, Downloaded from https://agupubs.onlinelibrary.wiley.com/doi/10.1029/2024GL114362 by Universidad Complutense De Madrid, Wiley Online Library on [09/02/2026]. See the Terms and Conditions (https://onlinelibrary.wiley.com/terms-and-conditions) on Wiley Online Library for rules of use; OA articles are governed by the applicable Creative Commons License

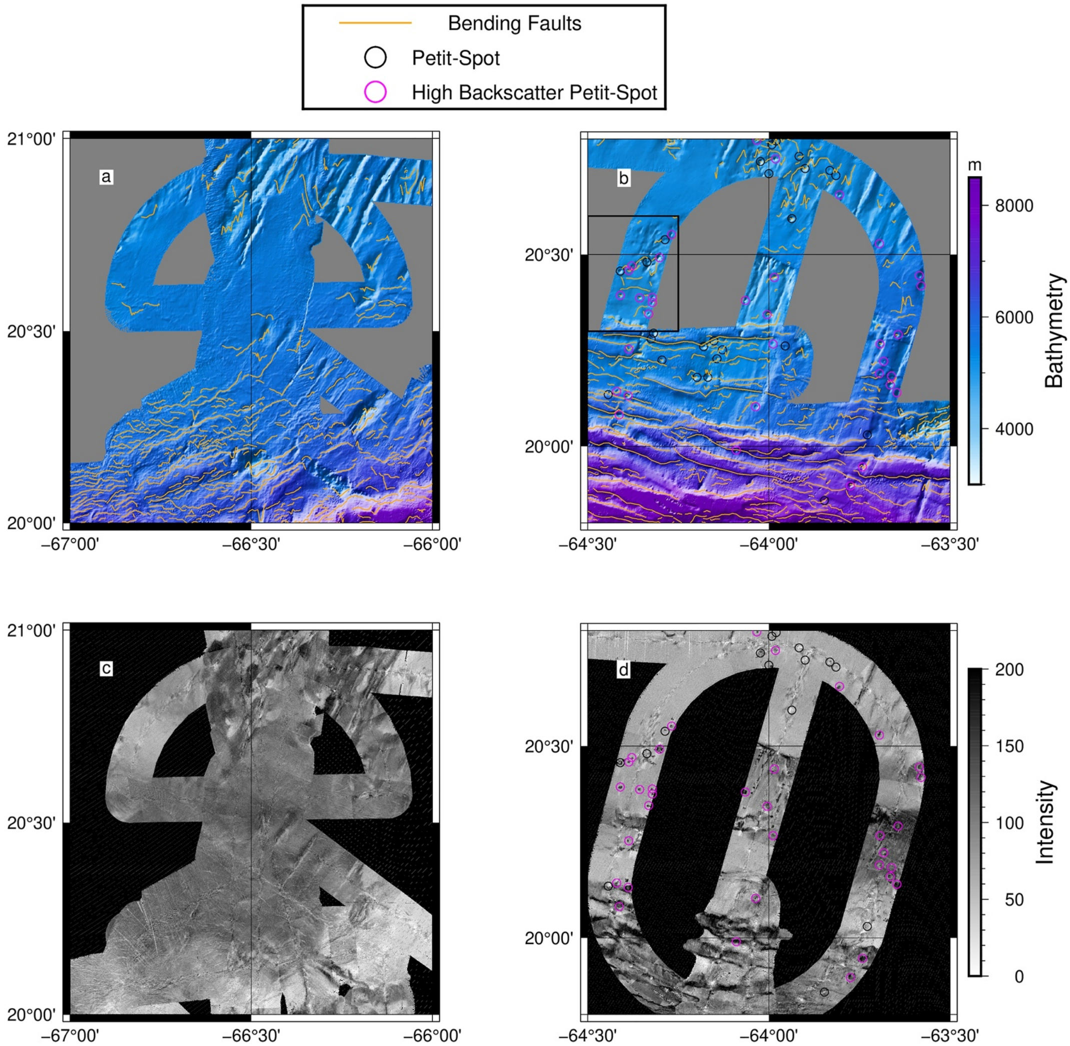

Figure 3. Zoom of western and eastern section bathymetry and backscatter intensity. (a) Bathymetry of the outer rise of the western section (b) Bathymetry of the outer rise of the eastern section. Black circles indicate knolls or petit spots with low backscatter intensity (<100), while magenta circles indicate knolls or petit spots with high backscatter intensity (>100). Black box indicates the general location shown in detail in Figure 4. (c) Backscatter of the outer rise of the western section. (d) Backscatter of the outer rise of the eastern section.

Hirano et al., 2006). Additional observations of volcanism have been made on the shallower concave downward portions of the outer rise, and these samples are thought to rapidly traverse the lithosphere (Hirano et al., 2008; Sato et al., 2018), with little contamination. Their rapid ascent is attributed to the dominantly extensional regime of the peak of the outer rise (Hirano & Machida, 2022). The locations of the knolls in the PRT are akin to those found on top of the outer rise elsewhere. However, there are several high backscatter seamounts that are on the outer trench wall. We cannot ascertain if the knolls erupted in situ on the trench wall or if they formed elsewhere on the outer rise and moved into the trench as has been proposed for the Japan Trench (Hirano et al., 2006). Age dates of the seamounts are needed to resolve this issue. Due to lack of high resolution bathymetric and backscatter data we also cannot preclude there is more volcanism seaward of the mapped area.

The stress regime in the PRT may be different than the other locations of petit-spot volcanism and may explain the tendency of the knolls to be located toward the trench. Specifically, there are a differences in the strength of the downgoing plate between PRT and the Japan Trench. The PRT has a smaller effective elastic thickness (~30 km vs. 56–62 km) (Levitt & Sandwell, 1995) even though the plate is >100 Myr old in both cases and should be of similar thickness (Hasterok, 2013; Stein & Stein, 1992). This results in a narrower positive FAA and outer rise

19448007, 2025, 10, Downloaded from https://agupubs.onlinelibrary.wiley.com/doi/10.1029/2024GL114362 by Universidad Complutense De Madrid, Wiley Online Library on [09/02/2026]. See the Terms and Conditions (https://onlinelibrary.wiley.com/terms-and-conditions) on Wiley Online Library for rules of use; OA articles are governed by the applicable Creative Commons License

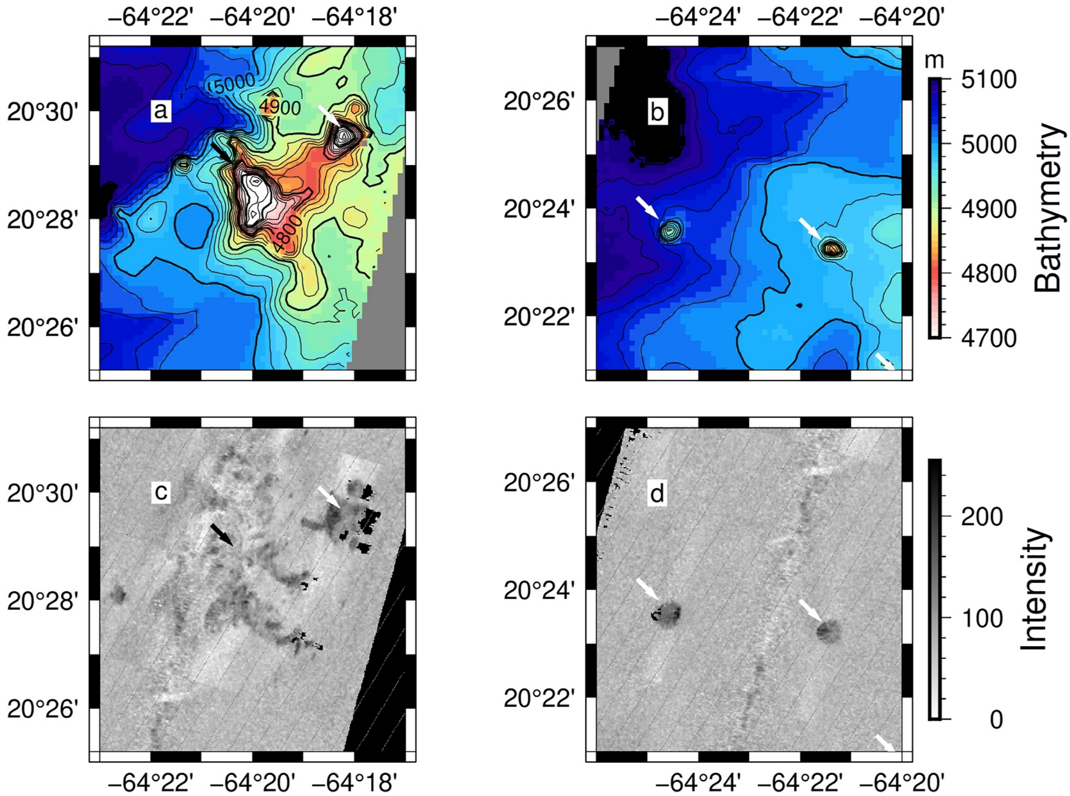

Figure 4. Zoom of high backscatter knolls in eastern section. (a) Bathymetry of amorphous knoll exhibiting relatively low backscatter (black arrow) and knoll with high backscatter (white arrow). (b) Bathymetry of high backscatter knolls formed in relatively flat sedimented seafloor (white arrows). (c) Backscatter intensity for the region in panels (a) and (d) backscatter intensity for region shown in panel (b).

here (~100 km) relative to the Japan Trench (~400 km) (Bassett & Watts, 2015). The thinner than expected plate may also be indicative of plate buckling especially considering the larger scarps found in the eastern section presented here and in previous work (ten Brink, 2005). The stress regime and narrower outer rise may focus melts preferentially toward the trench side of the rise.

There are two explanations for why we see petit spot volcanism in the east rather than the west: possible differences in stress regime along strike and/or heterogeneous distribution of melt at the LAB. These explanations are not mutually exclusive.

Our fault scarp analysis and other lines of evidence suggest there are changes in stress regime along strike of the PRT. There are differences between the bending fault scarps in the western and eastern section of the PRT in terms of fault scarp azimuth, length and height as well as the evidence for young volcanism. The western section has scarps with shorter length and height, a broader range of azimuths, and no evidence for young volcanism. The eastern section has longer scarps with greater heights. The scarps are preferentially aligned subparallel to E-W and to the fracture zone trends. The positive FAA in the east also encompasses several large faults suggesting the faulting is established in the concave downward part of the outer rise. The larger and longer scarps in the eastern section suggest the existence of larger bending stresses (extensional) here and/or pre-existing zones of weakness due to the Vidal (Jacksonville) fracture zone. The difference in stress between the sections is supported by the larger number of seismic events >M 2.5 over the past 50 years in the outer rise region observed in the eastern section than in the western section (189 vs. 119, Figure 1c) (USGS, 2024). Also, tsunami deposits in the British Virgin Islands are consistent with a pre-Columbian (~600 years ago) M 8.17 outer rise earthquake in the eastern section (although a megathrust source is also possible) (Wei et al., 2024). We speculate that the difference in stresses and zones of weakness between the east and west may make magma escaping from the asthenospheric mantle through the lithosphere more likely in one section over the other. Further work is needed to determine if the differences in stress are significant enough to allow melt to escape in the east versus the west.

19448007, 2025, 10, Downloaded from https://agupubs.onlinelibrary.wiley.com/doi/10.1029/2024GL114362 by Universidad Complutense De Madrid, Wiley Online Library on [09/02/2026]. See the Terms and Conditions (https://onlinelibrary.wiley.com/terms-and-conditions) on Wiley Online Library for rules of use; OA articles are governed by the applicable Creative Commons License

19448007, 2025, 10, Downloaded from https://agupubs.onlinelibrary.wiley.com/doi/10.1029/2024GL114362 by Universidad Complutense De Madrid, Wiley Online Library on [09/02/2026]. See the Terms and Conditions (https://onlinelibrary.wiley.com/terms-and-conditions) on Wiley Online Library for rules of use; OA articles are governed by the applicable Creative Commons License

The varied existence of petit-spots in our study region may also be explained by heterogeneous distribution of partial melt at the LAB. The heterogeneity of partial melt at the LAB globally has been suggested by active source seismic imaging (Mehouachi & Singh, 2018), passive seismic (Harmon et al., 2020; Rychert et al., 2021; Saikia et al., 2021) and magnetotelluric imaging (Wang et al., 2020) at the equatorial Mid-Atlantic Ridge from 0 to 80 Myr old seafloor where melt is imaged in discrete locations. The melt may also preferentially pond beneath thinner and or topographically shallower lithosphere (Hirano & Machida, 2022) as suggested by modeling of two-phase flow (Sim et al., 2020; Turner et al., 2017). Shallowing of the LAB may occur during plate flexure (Hirano et al., 2006; Hirano & Machida, 2022) or by small scale convective processes, which have been observed on younger seafloor (Harmon et al., 2020; Rychert et al., 2021; Saikia et al., 2021). The single S-to-P receiver function imaging study of the LAB in the region does not see evidence for a sharp LAB beneath the incoming plate in the PRT (Possee et al., 2021) that could be caused by the presence of partial melt. The study had limited resolution at <70 km depth beneath the incoming plate, so the melt could exist at these shallow depths. Alternatively, if the lithosphere is 80–100 km thick north of the PRT as imaged offshore Hispaniola (Possee et al., 2021), there may be not be a S-to-P converted phase generated by partial melt at the LAB. In this case, the volcanism may have effectively drained the melt at the LAB and reduced the velocity contrast. Establishing the relationship between the deeper mantle structure and whether partial melt exists in discrete regions in the asthenosphere beneath the outer rise will be important for understanding the distribution of petit-spot volcanism in the PRT and elsewhere.

5. Conclusion

We present evidence for recent petit-spot volcanism on the outer rise of the PRT, based on the interpretation of high backscatter intensity volcanic cones in multibeam bathymetric data. The volcanism is found only in the eastern section of the PRT, east of 65.9°W longitude, where bending fault scarps are longest and highest in the region. We speculate that the inferred higher stress regime of the outer rise in this region facilitates the escape of asthenospheric magmas to form the petit-spot volcanism in the eastern section. In addition, the melt supply may be varied along strike with no melt available at the LAB in the western section. Future work sampling the newly mapped knolls is needed to verify if these bathymetric features are due to recent petit-spot volcanism. The chemistry of the petit-spot volcanos may elucidate the nature of the "background" asthenosphere beneath the Atlantic and help determine if there are fundamental differences between the Pacific and Atlantic mantle systems.

Data Availability Statement

The multibeam data used for the bathymetric and backscatter intensity analysis in the study are available at the National Centers for Environmental Information (NOAA, 2024) via Canales (2023) and ten Brink (2023).

Acknowledgments
The authors acknowledge funding from NSF-OCE 2309734. We also thank the captains and crew of the RV Marcus G. Langseth for their assistance during MGL2314, MGL2315, and MGL2316. We thank Naoto Hirano and an anonymous reviewer for their thoughtful and constructive reviews. Any use of trade, firm, or product names is for descriptive purposes only and does not imply endorsement by the U.S. Government.

References

Akizawa, N., Hirano, N., Matsuzaki, K. M., Machida, S., Tamura, C., Kaneko, J., et al. (2022). A direct evidence for disturbance of whole sediment layer in the subducting Pacific plate by petit-spot magma–water/sediment interaction. *Marine Geology*, *444*, 106712. https://doi.org/10.1016/j.margeo.2021.106712

Altamimi, Z., Métivier, L., Rebischung, P., Collilieux, X., Chanard, K., & Barnéoud, J. (2023). ITRF2020 plate motion model. *Geophysical Research Letters*, *50*(24), e2023GL106373. https://doi.org/10.1029/2023GL106373

Andrews, B. D., ten Brink, U. S., Danforth, W. W., Chaytor, J. D., Granja-Bruna, J., & Carbo-Gorosabel, A. (2014). *Bathymetric terrain model of the Puerto Rico trench and the northeastern Caribbean region for marine geological investigations* [Report] (2013-1125). (Open-File report, issue). U. S. Geological Survey. Retrieved from https://pubs.usgs.gov/publication/ofr20131125

Antonov, J. I., Seidov, D., Boyer, T. P., Locarnini, R. A., Mishonov, A. V., Garcia, H. E., et al. (2010). In S. Levitus (Ed.), *World Ocean atlas 2009, volume 2: Salinity* (Vol. 69, p. 184). NOAA Atlas NESDIS.

Bassett, D., & Watts, A. B. (2015). Gravity anomalies, crustal structure, and seismicity at subduction zones: 1. Seafloor roughness and subducting relief. *Geochemistry, Geophysics, Geosystems*, *16*(5), 1508–1540. https://doi.org/10.1002/2014gc005684

Bunce, E. T., & Fahlquist, D. A. (1962). Geophysical investigation of the Puerto Rico trench and outer ridge. *Journal of Geophysical Research*, *67*(10), 3955–3972. https://doi.org/10.1029/JZ067i010p03955

Canales, J. P. (2023). Puerto Rico Trench OBS [Dataset]. *Rolling Deck 2 Repository*. https://doi.org/10.7284/910269

Canny, J. (1986). A computational approach to edge detection. *IEEE Transactions on Pattern Analysis and Machine Intelligence*, *PAMI-8*(6), 679–698. https://doi.org/10.1109/TPAMI.1986.4767851

DeMets, C., Gordon, R. G., & Argus, D. F. (2010). Geologically current plate motions. *Geophysical Journal International*, *181*(1), 1–80. https://doi.org/10.1111/j.1365-246X.2009.04491.x

Ewing, J., & Ewing, M. (1962). Reflection profiling in and around the Puerto Rico Trench. *Journal of Geophysical Research*, *67*(12), 4729–4739. https://doi.org/10.1029/JZ067i012p04729

Forsyth, D. W. (1992). Geophysical constraints on mantle flow and melt generation beneath mid-ocean ridges. In J. Phipps Morgan, D. K. Blackman, & J. M. Sinton (Eds.), *Mantle flow and melt generation at mid-ocean ridges*, *Geophysical Monograph Series* (Vol. 71, pp. 1–65). AGU. https://doi.org/10.1029/gm071p0001

French, C. D., & Schenk, C. J. (2004). Map showing geology, oil and gas fields, and geologic provinces of the Caribbean Region.
Fujiwara, T., Hirano, N., Abe, N., & Takizawa, K. (2007). Subsurface structure of the "petit-spot" volcanoes on the northwestern Pacific Plate. *Geophysical Research Letters*, *34*(13), L13305. https://doi.org/10.1029/2007GL030439
Harigane, Y., Mizukami, T., Morishita, T., Michibayashi, K., Abe, N., & Hirano, N. (2011). Direct evidence for upper mantle structure in the NW Pacific Plate: Microstructural analysis of a petit-spot peridotite xenolith. *Earth and Planetary Science Letters*, *302*(1), 194–202. https://doi.org/10.1016/j.epsl.2010.12.011
Harmon, N., Rychert, C. A., Kendall, J. M., Agius, M., Bogiatzis, P., & Tharimena, S. (2020). Evolution of the oceanic lithosphere in the equatorial Atlantic from Rayleigh wave tomography, evidence for small-scale convection from the PI-LAB experiment. *Geochemistry, Geophysics, Geosystems*, *21*(9), e2020GC009174. https://doi.org/10.1029/2020GC009174
Hasterok, D. (2013). A heat flow based cooling model for tectonic plates. *Earth and Planetary Science Letters*, *361*, 34–43. https://doi.org/10.1016/j.epsl.2012.10.036
Hirano, N. (2011). Petit-spot volcanism: A new type of volcanic zone discovered near a trench. *Geochemical Journal*, *45*(2), 157–167. https://doi.org/10.2343/geochemj.1.0111
Hirano, N., Koppers, A. A. P., Takahashi, A., Fujiwara, T., & Nakanishi, M. (2008). Seamounts, knolls and petit-spot monogenetic volcanoes on the subducting Pacific Plate. *Basin Research*, *20*(4), 543–553. https://doi.org/10.1111/j.1365-2117.2008.00363.x
Hirano, N., & Machida, S. (2022). The mantle structure below petit-spot volcanoes. *Communications Earth & Environment*, *3*(1), 110. https://doi.org/10.1038/s43247-022-00438-1
Hirano, N., Machida, S., Abe, N., Morishita, T., Tamura, A., & Arai, S. (2013). Petit-spot lava fields off the central Chile trench induced by plate flexure. *Geochemical Journal*, *47*(2), 249–257. https://doi.org/10.2343/geochemj.2.0227
Hirano, N., Machida, S., Sumino, H., Shimizu, K., Tamura, A., Morishita, T., et al. (2019). Petit-spot volcanoes on the oldest portion of the Pacific plate. *Deep Sea Research Part I: Oceanographic Research Papers*, *154*, 103142. https://doi.org/10.1016/j.dsr.2019.103142
Hirano, N., Takahashi, E., Yamamoto, J., Abe, N., Ingle, S. P., Kaneoka, I., et al. (2006). Volcanism in response to plate flexure. *Science*, *313*(5792), 1426–1428. https://doi.org/10.1126/Science.1128235
Kim, Y.-S., & Sanderson, D. J. (2005). The relationship between displacement and length of faults: A review. *Earth-Science Reviews*, *68*(3), 317–334. https://doi.org/10.1016/j.earscirev.2004.06.003
Klein, E. M., & Langmuir, C. H. (1987). Global correlations of ocean ridge basalt chemistry with axial depth and crustal thickness. *Journal of Geophysical Research*, *92*(8), 8089–8115. https://doi.org/10.1029/JB092iB08p08089
Levitt, D. A., & Sandwell, D. T. (1995). Lithospheric bending at subduction zones based on depth soundings and satellite gravity. *Journal of Geophysical Research*, *100*(B1), 379–400. https://doi.org/10.1029/94jb02468
Levitus, S. (1982). Climatological atlas of the world ocean, *NOAA/ERL GFDL Professional Paper 13* (NTIS PB183-184093) (p. 173).
Locarnini, R. A., Mishonov, A. V., Antonov, J. I., Boyer, T. P., Garcia, H. E., Baranova, O. K., et al. (2010). World Ocean atlas 2009, volume 1: Temperature. In S. Levitus (Ed.), *NOAA Atlas NESDIS* (Vol. 68, p. 184). U.S. Government Printing Office.
Machida, S., Kogiso, T., & Hirano, N. (2017). Petit-spot as definitive evidence for partial melting in the asthenosphere caused by CO_2. *Nature Communications*, *8*(1), 14302. https://doi.org/10.1038/ncomms14302
Masson, D. G., & Scanlon, K. M. (1991). The neotectonic setting of Puerto Rico. *GSA Bulletin*, *103*(1), 144–154. https://doi.org/10.1130/0016-7606
Matthews, K. J., Maloney, K. T., Zahirovic, S., Williams, S. E., Seton, M., & Muller, D. (2016). Global plate boundary evolution and kinematics since the late Paleozoic. *Global and Planetary Change*, *146*, 226–250. https://doi.org/10.1016/j.gloplacha.2016.10.002
Mehouachi, F., & Singh, S. (2018). Water-rich sublithospheric melt channel in the equatorial Atlantic Ocean. *Nature Geoscience*, *11*(1), 65–69. https://doi.org/10.1038/s41561-017-0034-z
Mikuni, K., Hirano, N., Akizawa, N., Yamamoto, J., Machida, S., Tamura, A., et al. (2022). Lithological structure of western Pacific lithosphere reconstructed from mantle xenoliths in a petit-spot volcano. *Progress in Earth and Planetary Science*, *9*(1), 62. https://doi.org/10.1186/s40645-022-00518-y
Morgan, W. J. (1971). Convection plumes in the lower mantle. *Nature*, *230*(5288), 42–43. https://doi.org/10.1038/230042a0
Muller, R. D., Sdrolias, M., Gaina, C., & Roest, W. R. (2008). Age, spreading rates, and spreading asymmetry of the world's ocean crust. *Geochemistry, Geophysics, Geosystems*, *9*(4), Q04006. https://doi.org/10.1029/2007gc001743
Naif, S., Key, K., Constable, S., & Evans, R. L. (2013). Melt-rich channel observed at the lithosphere-asthenosphere boundary. *Nature*, *495*(7441), 356–359. https://doi.org/10.1038/nature11939
NOAA. (2024). National Centers for Environmental Information. Retrieved from https://www.ngdc.noaa.gov/mgg/
Ohira, A., Kodaira, S., Fujie, G., No, T., Nakamura, Y., Kaiho, Y., & Miura, S. (2018). Seismic structure of the oceanic crust around petit-spot volcanoes in the outer-rise region of the Japan trench. *Geophysical Research Letters*, *45*(20), 11123–11129. https://doi.org/10.1029/2018GL080305
Okumura, S., & Hirano, N. (2013). Carbon dioxide emission to Earth's surface by deep-sea volcanism. *Geology*, *41*(11), 1167–1170. https://doi.org/10.1130/g34620.1
Peretyazhko, I. S., Savina, E. A., & Pulyaeva, I. A. (2024). Miocene petit-spot basanitic volcanoes on Cretaceous Alba Guyot (Magellan Seamount Trail, Pacific Ocean). *Geosciences*, *14*(10), 252. https://doi.org/10.3390/geosciences14100252
Pilet, S., Abe, N., Rochat, L., Kaczmarek, M. A., Hirano, N., Machida, S., et al. (2016). Pre-subduction metasomatic enrichment of the oceanic lithosphere induced by plate flexure. *Nature Geoscience*, *9*(12), 898–903. https://doi.org/10.1038/Ngeo2825
Possee, D., Rychert, C., Harmon, N., & Keir, D. (2021). Seismic discontinuities across the North American Caribbean Plate boundary from S-to-P receiver functions. *Geochemistry, Geophysics, Geosystems*, *22*(7), e2021GC009723. https://doi.org/10.1029/2021GC009723
Rychert, C. A., Harmon, N., Constable, S., & Wang, S. (2020). The nature of the lithosphere-Asthenosphere boundary. *Journal of Geophysical Research: Solid Earth*, *125*(10), e2018JB016463. https://doi.org/10.1029/2018jb016463
Rychert, C. A., & Shearer, P. (2011). Imaging the lithosphere-asthenosphere boundary beneath the Pacific using SS waveform modeling. *Journal of Geophysical Research*, *116*(7), B07307. https://doi.org/10.1029/2010JB008070
Rychert, C. A., Tharimena, S., Harmon, N., Wang, S., Constable, S., Kendall, J. M., et al. (2021). A dynamic lithosphere-asthenosphere boundary near the equatorial Mid-Atlantic Ridge. *Earth and Planetary Science Letters*, *566*, 116949. https://doi.org/10.1016/j.epsl.2021.116949
Saikia, U., Rychert, C., Harmon, N., & Kendall, J. M. (2021). Upper mantle anisotropic shear velocity structure at the equatorial Mid-Atlantic Ridge constrained by Rayleigh wave group velocity analysis from the PI-LAB experiment. *Geochemistry, Geophysics, Geosystems*, *22*(3), e2020GC009495. https://doi.org/10.1029/2020GC009495
Sandwell, D. T., Muller, R. D., Smith, W. H. F., Garcia, E., & Francis, R. (2014). New global marine gravity model from CryoSat-2 and Jason-1 reveals buried tectonic structure. *Science*, *346*(6205), 65–67. https://doi.org/10.1126/science.1258213

19448007, 2025, 10, Downloaded from https://agupubs.onlinelibrary.wiley.com/doi/10.1029/2024GL114362 by Universidad Complutense De Madrid, Wiley Online Library on [09/02/2026]. See the Terms and Conditions (https://onlinelibrary.wiley.com/terms-and-conditions) on Wiley Online Library for rules of use; OA articles are governed by the applicable Creative Commons License

Sandwell, D. T., Winterer, E. L., Mammerickx, J., Duncan, R. A., Lynch, M. A., Levitt, D. A., & Johnson, C. L. (1995). Evidence for diffuse extension of the Pacific Plate from Pukapuka ridges and cross-grain gravity lineations. *Journal of Geophysical Research*, *100*(8), 15087–15099. https://doi.org/10.1029/95jb00156

Sato, Y., Hirano, N., Machida, S., Yamamoto, J., Nakanishi, M., Ishii, T., et al. (2018). Direct ascent to the surface of asthenospheric magma in a region of convex lithospheric flexure. *International Geology Review*, *60*(10), 1231–1243. https://doi.org/10.1080/00206814.2017.1379912

Sim, S. J., Spiegelman, M., Stegman, D. R., & Wilson, C. (2020). The influence of spreading rate and permeability on melt focusing beneath mid-ocean ridges. *Physics of the Earth and Planetary Interiors*, *304*, 106486. https://doi.org/10.1016/j.pepi.2020.106486

Stein, C. A., & Stein, S. (1992). A model for the global variation in oceanic depth and heat flow with lithospheric age. *Nature*, *359*(6391), 123–129. https://doi.org/10.1038/359123a0

Stern, R. L., (2002). Subduction zones. *Rev. of Geophys.*, *40*(4), 3-1–3-38. https://doi.org/10.1029/2001RG000108

Symithe, S., Calais, E., de Chabalier, J. B., Robertson, R., & Higgins, M. (2015). Current block motions and strain accumulation on active faults in the Caribbean. *Journal of Geophysical Research: Solid Earth*, *120*(5), 3748–3774. https://doi.org/10.1002/2014JB011779

Taneja, R., Rushmer, T., Blichert-Toft, J., Turner, S., & O'Neill, C. (2016). Mantle heterogeneities beneath the Northeast Indian Ocean as sampled by intra-plate volcanism at Christmas Island. *Lithos*, *262*, 561–575. https://doi.org/10.1016/j.lithos.2016.07.027

ten Brink, U. (2005). Vertical motions of the Puerto Rico Trench and Puerto Rico and their cause. *Journal of Geophysical Research*, *110*(B6), B06404. https://doi.org/10.1029/2004JB003459

ten Brink, U. (2023). Puerto Rico Trench MCS. [Dataset]. *Rolling Deck 2 Repository*. https://doi.org/10.7284/910268

ten Brink, U., Danforth, W., Polloni, C., Andrews, B., Llanes, P., Smith, S., et al. (2004). New seafloor map of the Puerto Rico Trench helps assess earthquake and tsunami hazards. *Eos Transactions American Geophysical Union*, *85*(37), 349–360. https://doi.org/10.1029/2004EO370001

Torabi, A., & Berg, S. S. (2011). Scaling of fault attributes: A review. *Marine and Petroleum Geology*, *28*(8), 1444–1460. https://doi.org/10.1016/j.marpetgeo.2011.04.003

Turner, A. J., Katz, R. F., Behn, M. D., & Keller, T. (2017). Magmatic focusing to mid-ocean ridges: The role of grain-size variability and non-Newtonian viscosity. *Geochemistry, Geophysics, Geosystems*, *18*(12), 4342–4355. https://doi.org/10.1002/2017gc007048

USGS. (2024). Advanced Nations Seismic System (ANSS) comprehensive catalog of earthquake events and products. https://doi.org/10.5066/F7MS3QZH

Wang, S., Constable, S., Rychert, C. A., & Harmon, N. (2020). A lithosphere-asthenosphere boundary and partial melt estimated using marine magnetotelluric data at the central middle Atlantic ridge. *Geochemistry, Geophysics, Geosystems*, *21*(9), e2020GC009177. https://doi.org/10.1029/2020GC009177

Wei, Y., ten Brink, U. S., & Atwater, B. F. (2024). Modeled flooding by tsunamis and a storm versus observed extent of coral erratics on Anegada, British Virgin Islands—Further evidence for a great Caribbean earthquake six centuries ago. *Journal of Geophysical Research: Solid Earth*, *129*(3), e2023JB028387. https://doi.org/10.1029/2023JB028387

Wessel, P. (1989). Xover: A cross-over error detector for track data. *Computers and Geosciences*, *15*(3), 333–346. https://doi.org/10.1016/0098-3004(89)90044-7

Yamamoto, J., Korenaga, J., Hirano, N., & Kagi, H. (2014). Melt-rich lithosphere-asthenosphere boundary inferred from petit-spot volcanoes. *Geology*, *42*(11), 967–970. https://doi.org/10.1130/g35944.1

19448007, 2025, 10, Downloaded from https://agupubs.onlinelibrary.wiley.com/doi/10.1029/2024GL114362 by Universidad Complutense De Madrid, Wiley Online Library on [09/02/2026]. See the Terms and Conditions (https://onlinelibrary.wiley.com/terms-and-conditions) on Wiley Online Library for rules of use; OA articles are governed by the applicable Creative Commons License